





Submillimeter Signatures from Growing Supermassive Black Holes before Reionization

Evgenii O. Vasiliev^{1,2}  and Yuri A. Shchekinov^{2,3} ¹ Southern Federal University, Rostov on Don 344090, Russia; eugstar@mail.ru² Lebedev Physical Institute, Russian Academy of Sciences, 53 Leninsky Ave., Moscow 119991, Russia³ Raman Research Institute, Sadashivanagar, Bengaluru 560080, Karnataka, India

Received 2019 July 28; revised 2019 November 3; accepted 2019 November 5; published 2019 December 18

Abstract

The presence of supermassive black holes (SMBHs) with masses up to $M_{\bullet} \sim 10^9 M_{\odot}$ at redshifts $z \simeq 7.5$ suggests that their seeds may have started to grow long before the reionization in ambient medium with pristine chemical composition. During their latest 500 Myr episode of growing from $z \geq 10$ to $z \sim 7$, the black holes shone as luminous as $10^{11} - 10^{12} L_{\odot}$, with a cumulative spectrum consisting of the intrinsic continuum from the hot accretion disk, nebular hydrogen, and helium spectral lines, and the free-free continuum from the gas of host halos. Here we address the question of whether such a plain spectrum would allow us to trace the evolution of these growing SMBHs. In our calculations we assume that host galaxies have stellar populations with masses smaller than the masses of their central black holes—the so-called obese black hole galaxies. Within this model we show that for a sufficiently high mass of gas in a host galaxy—not smaller than the mass of a growing black hole, the cumulative spectrum in the far-infrared reveals a sharp transition from a quasi-blackbody Rayleigh–Jeans spectrum of the black hole $\propto \lambda^{-2}$ to a flat free-free nebular continuum $\lambda^{0.118}$ on a longer wavelength limit. Once such a transition in the spectrum is resolved, the black hole mass can be inferred as a combination of the observed wavelength at the transition λ_k and the corresponding spectral luminosity. The possible observability of this effect in spectra of growing high- z SMBHs and determination of their mass with the upcoming *James Webb Space Telescope* and the planned space project Spektr-M is briefly discussed.

Unified Astronomy Thesaurus concepts: [Cosmology \(343\)](#); [Submillimeter astronomy \(1647\)](#); [Supermassive black holes \(1663\)](#)

1. Introduction

Supermassive black holes (SMBH) with masses $M_{\bullet} \sim 10^9 - 10^{10} M_{\odot}$ are recognized to be present at redshifts as high as $z \simeq 6 - 7.5$, when the universe was 650–800 Myr young (Fan et al. 2003; Willott et al. 2010; Mortlock et al. 2011; Bañados et al. 2014, 2018; Wu et al. 2015; Decarli et al. 2018; Izumi et al. 2019)—in total more than 150 such SMBHs are already known (see, e.g., Fan et al. 2019). Their origin remains elusive—it is unclear how massive their seeds were, how efficient their growth rate was, and what was the mass reservoir for their growth. To fit the existence of the quasars J0100 + 2802 ($z = 6.33$), J1120 + 0641 ($z = 7.09$), and J1342 + 0928 ($z = 7.54$) with SMBH masses $M_{\bullet} = 1.2 \times 10^{10}$, 2×10^9 , and $7.8 \times 10^8 M_{\odot}$ respectively, one has to assume that their masses grow as $M_{\bullet} = M_{\bullet,0} \exp [t/(47 \text{ Myr})]$, corresponding to the standard Eddington limit with a 10% radiative efficiency ϵ , the Salpeter growth time $t_S = \epsilon c \sigma_T / (4\pi G m_p) = 47 \text{ Myr}$, and the seed mass $M_{\bullet,0} \geq 10^3 M_{\odot}$ at $z \geq 40$ (Bañados et al. 2018). In this scenario SMBHs have to begin growing even earlier than the very first stars are assumed to have appeared (see discussion in Barkana & Loeb 2001). Moreover, it suggests that the accretion is tightly tuned to the Eddington rate, which seems physically unlikely (see discussion in Haiman & Loeb 2001; Volonteri & Rees 2005; Haiman 2013; Alexander & Natarajan 2014; Madau et al. 2014). Lower-mass black holes with $M_{\bullet} \sim 100 M_{\odot}$, originated from Population III stars, are apparently unlikely to serve as seeds for growing SMBHs, because photoionization and photoheating from their massive progenitors strongly suppress further supply of cold mass onto the BH (Johnson & Bromm 2007), and would require even more time for the black hole to grow. Note, however, that this channel for SMBH seeds is currently widely discussed (see references in Natarajan et al. 2019). Also note that this problem of

the presence of such enormously massive BHs in a younger than 1 Gyr universe can be to a certain extent eased when possible magnification of $z > 6$ SMBHs due to gravitational lensing is considered (Fan et al. 2019; Pacucci & Loeb 2019a, 2019b). Recent millimeter observations of the quasar J0100 + 2802 ($z = 6.33$) with the most massive BH, $M_{\bullet} \sim 1.2 \times 10^{10} M_{\odot}$, known at $z > 6$, indicate strong lensing with a magnification factor of ~ 450 (Fujimoto et al. 2019). As a result, the estimate of the SMBH mass may be reduced by more than an order of magnitude, though this still remains exceedingly large for a 1 Gyr universe $\sim 10^9 M_{\odot}$ (Fujimoto et al. 2019). The fraction of so strongly magnified quasars is fairly low considering the very small typical angular size of such lenses, as a rule $\ll 1''$ (see, e.g., Pei 1995; Bolton et al. 2008; Pacucci & Loeb 2019b).

More suitable scenarios can involve (i) a hierarchical assembly of pregalactic massive black holes in Λ CDM cosmology (Volonteri et al. 2003; Madau et al. 2004; Yoo & Miralda-Escude 2004; Volonteri & Rees 2005), (ii) rapid growth of massive BHs with highly supercritical rates (Volonteri et al. 2015), involving in particular a supercritical “slim” disk mode (Begelman & Meier 1982; Paczynski & Abramowicz 1982; Abramowicz et al. 1988; Madau et al. 2014) or a “supra-exponential” growth of a low-mass stellar BH in a very dense environment with a low-angular-momentum velocity field (Alexander & Natarajan 2014), (iii) a direct-collapse black hole (DCBH) of intermediate mass ($\sim 10^4 - 10^5 M_{\odot}$) growing in a gaseous halo with a low-mass stellar population (lower than the DCBH mass at the beginning of their common evolution Volonteri et al. 2008; Natarajan et al. 2017)—the obese black hole galaxy (OBG) stage, as termed by Agarwal et al. (2013). The first two scenarios suggest a stochastic super-Eddington feeding by high-density

regions in the host galaxies and rapid growth in later epochs $z_0 \lesssim 20$. The third scenario requires more massive stellar seeds than low-mass stellar seeds present, presumably in a population of halos hosting intermediate-mass BHs ($M_* \lesssim 10^5 M_\odot$) grown at earlier epochs $z \gtrsim 20$ under a fast DCBH growth (see discussion in Haehnelt & Rees 1993; Bromm & Loeb 2003; Yoshida et al. 2003; Lodato & Natarajan 2006; Visbal et al. 2014a, 2014b; Agarwal et al. 2016; Chon et al. 2016; Pacucci et al. 2016, 2017; Latif & Ferrara 2016; Inayoshi et al. 2018; Maio et al. 2018; Wise et al. 2019). To discriminate between these scenarios, observations of SMBHs at even higher redshifts $z > 7.5$, closer to the beginning of their growth, are needed. Moreover, taking into account the case of the quasar J0100 + 2802 multiwavelength observations would help put constraints on the early phases of SMBH growth (see the recent discussion in Fan et al. 2019; Fujimoto et al. 2019; Pacucci & Loeb 2019b).

All scenarios predict the presence of higher-mass BHs growing from $M_* \sim 10^5$ to $\sim 10^9 M_\odot$ between redshifts $z = 20$ and $z \simeq 8$. In the Eddington regime their bolometric luminosities lie in the range $L_{\text{Edd}} \sim 10^{43} - 10^{47} \text{ erg s}^{-1}$. For a medium spectral resolution $R \sim 1000$ the expected flux density is of $S_\nu \sim 0.01 - 100 \mu\text{Jy}$ in the infrared band $\lambda \sim 1 \mu\text{m}$ ($\nu \sim 300 \text{ THz}$) (for more discussion see Natarajan et al. 2017) and $\sim 1 \mu\text{Jy}$ to 0.1 Jy in the submillimeter band $\nu \sim 300 \text{ GHz}$ ($\lambda \sim 0.1 \text{ mm}$) (see, e.g., Valiante et al. 2018), respectively, compared to those measured in already discovered high-redshift SMBHs (Fan et al. 2003; Willott et al. 2010; Bañados et al. 2014, 2018). As such they can be detected by current and upcoming instruments. Several attempts to model fluxes from growing BHs in near-infrared and mid-infrared and their observational feasibility with the *James Webb Space Telescope* (*JWST*) were made by Pacucci et al. (2016), Natarajan et al. (2017), and Barrow et al. (2018). However, as far as possible longer-wavelength features (such as higher subordinate hydrogen line series, or free-free continuum) from even earlier phases of BH growth beyond $z > 10$ are concerned, the *JWST* capabilities can become inapplicable for detection of spectral manifestations from low-metallicity or pristine gas.

In this paper we address the question of whether observational signatures from growing BHs in epochs covered by redshifts between $z = 20$ and $z = 7.7$ can be observed in far-infrared and submillimeter wavebands, and whether the growing regime can be recognized from these manifestations. We argue that besides traditional line spectroscopy, spectral features in infrared and far-infrared continuum might be an efficient complementary tool for studying physical conditions in gas ionized and heated by a growing massive BH and the characteristics of the BH itself.

In the next section the model we use in our calculations is described: the accretion mode, the models of the BH and stellar population emission spectra and their interrelation. Section 3.1 contains the results: the evolution of the line and the continuum emissions from growing BHs and ionized ambient gas. In Section 4 we discuss issues related to the observability of growing BHs at redshifts $z > 7.5$ with the planned IR telescopes. Section 5 summarizes the results.

2. Model Description

2.1. Growth of the Black Hole

The red line in Figure 1 depicts an illustrative scenario with a continuous exponential growth rate $\dot{M} \propto M$ (Volonteri et al.

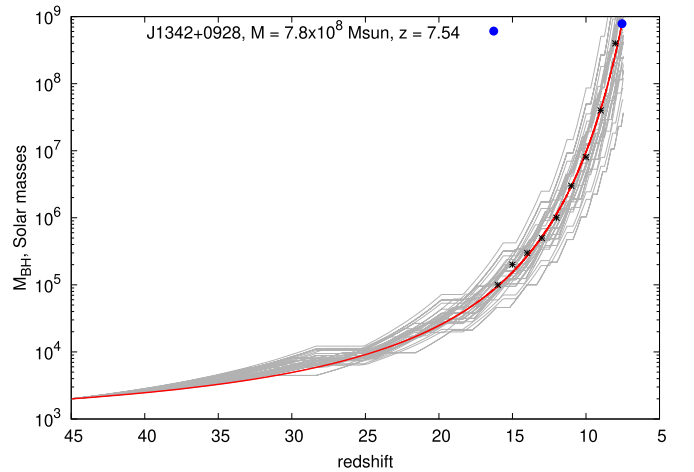


Figure 1. Black hole growth model. The blue point (solid circle) corresponds to the quasar J1342 + 0928 ($z = 7.54$) (Bañados et al. 2018), and the gray lines show the trajectories of growing BH masses from Equation (2) for different sets of t_i , η_i , and ϵ_i constrained by the condition $M(z = 8 \pm 1.5) = 3 \times 10^8 M_\odot$. The red line shows the average BH mass growth law, and the black dots around the red line indicate the black hole masses for which we calculate the spectra. The black points present one of the trajectories.

2003; Shapiro 2005; Madau et al. 2014) with the critical (Eddington) regime

$$M(t) = M_0 \exp\left(\frac{1 - \epsilon}{\epsilon} \frac{t}{0.47 \text{ Gyr}}\right) \quad (1)$$

where $M_0 = 1.6 \times 10^3 M_\odot$ at $z \geq 40$ and $\epsilon = 0.095$ is a mass-to-energy conversion factor (Soltan 1982; Volonteri et al. 2003) are assumed for $M(t)$ to reach $M_* = 7.8 \times 10^8 M_\odot$ at $z = 7.5$ as supposed by Bañados et al. (2018). This regime suggests a mass source that enhances its efficiency to a continuously tuned feeding equivalent to the critical accretion rate $\dot{M} \propto L_{\text{Edd}} \propto M(t)$, where L_{Edd} is the Eddington luminosity. A more realistic scenario can imply sporadic enhancement of the accretion rate to the super-Eddington level and subsequent quiet episodes, such that when averaged over large time the accretion corresponds to the regime resulting in a $10^9 M_\odot$ class black hole at $z \simeq 7$ (Madau et al. 2014; Pacucci et al. 2017). For these reasons we consider another model with episodically enhanced accretion from radiatively inefficient disks with a faster growth rate $\dot{M}_i(z)$:

$$\dot{M}(t) = \sum_i \frac{\eta_i(1 - \epsilon_i)}{\epsilon_i} \frac{M_i}{0.45 \text{ Gyr}} \Theta(t), \quad (2)$$

where

$$\Theta(t) = \begin{cases} 1, & t_i \leq t \leq t_i + \Delta t_i \\ 0, & \text{otherwise,} \end{cases}$$

with $M_i = M(t_i)$ being the mass reached during the i th episode of accretion; $\eta_i = L_i/L_{\text{Edd}} \gtrsim 1$ being a random number chosen in the limits $\eta_1 < \eta < \eta_2$ to ensure the mean mass of a grown BH $M_* = 3 \times 10^8 M_\odot$ at $z = 8$, which closely fits masses of observed BHs at $z = 7.5$, $\epsilon_i = \epsilon \lesssim 0.095$ is assumed; and t_i and Δt_i are chosen to match $\langle M(t) \rangle$ to $M_* = 3 \times 10^8 M_\odot$ at $z = 8$, as depicted by the red line in Figure 1. Furthermore, we calculate the spectra for one of the trajectories depicted in

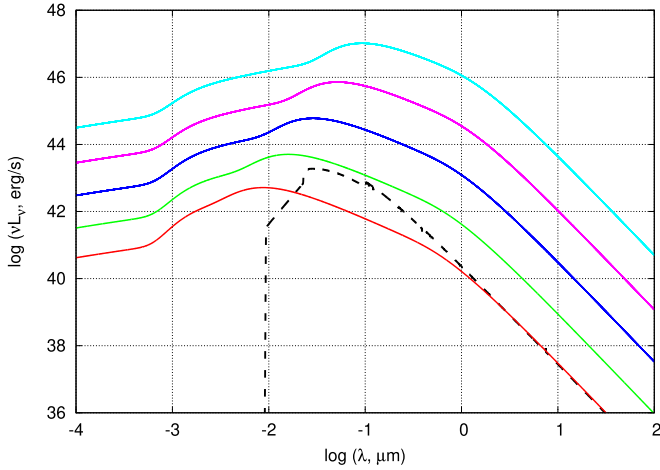


Figure 2. SEDs for BHs with masses 10^5 , 10^6 , 10^7 , 10^8 , and $10^9 M_\odot$ (solid color lines from bottom to top); clearly seen is the soft X-ray excess at $\lambda \sim 0.01\text{--}0.03 \mu\text{m}$ ($100\text{--}300 \text{ \AA}$), from the intermediate warm comptonizing region of the accretion disk (Kubota & Done 2018). The SED of the stellar bulge of a host galaxy as modeled by Zackrisson et al. (2011) for the metal-free stellar population Population III. One is shown by a dashed black line, and the red line shows spectra of central BHs with the mass $M \sim 0.02 M_*$ corresponding to the mass of the stellar population $M_* = 5 \times 10^6 M_\odot$.

Figure 1 with black points. With regard to the spectral features of growing BHs that we are aiming for here, one has to note that the models with randomly varying accretion (2) differ from the Eddington one (1) only by their observed fluxes versus the redshifts $z = z(F_\nu)$ corresponding to a given BH mass. In other words, once the redshift of a source is identified, the only relevant parameters are the spectral shape and the measured flux.

2.2. Spectrum of the Accreting BH

In our calculations we use a broadband spectral energy distribution (SED) of active galactic nuclei described by Kubota & Done (2018, 2019). It is based on the slim disk model (Abramowicz et al. 1988) of a radially stratified disk with three dominant regions: the hot inner disk extending from the innermost stable circular orbit R_{isco} to loosely defined edges of the hot Comptonizing region R_h , the warm Comptonizing region from R_h to R_w , and the outer region from R_w to R_{out} with a flat radial emissivity profile $F(r) \propto r^{-2}$ through over the disk. Within this model advection and wind outflow enhance radiation transfer and thus stabilize super-Eddington disks against the radiation-driven instability typical for standard disks with an exceeding luminosity (Kubota & Done 2018). The warm intermediate-disk region produces the soft X-ray excess (Kubota & Done 2018, 2019) contributing to the ionization and heating of the interstellar gas (see below) and consequently the nebular spectrum. The bolometric luminosity is assumed to be equal to the Eddington luminosity corresponding to the average value of the BH mass depicted by the solid red line in Figure 1: $L_{\text{Edd}} = 1.26 \times 10^{38} \langle M_*(t) \rangle \text{ erg s}^{-1}$, and $\langle M_* \rangle$ is in solar masses. Figure 2 presents several examples of SEDs for BHs with masses 10^5 , 10^6 , 10^7 , 10^8 , $10^9 M_\odot$ (from bottom to top).

2.3. Spectrum of the Stellar Population

For the stellar bulge SED shown in Figure 2 we utilized the population synthesis SED by Zackrisson et al. (2011) for the metal-free composite stellar population produced by a 30 Myr

long burst of Population III star formation (extremely top-heavy IMF: $50\text{--}500 M_\odot$, the Salpeter slope) with a constant rate.⁴ Note that such an extreme IMF has the highest contribution of stellar population into the domain of high-energy photons—X-ray and EUV, compared to other models: for instance, a Population II star with metallicity $[Z/H] \sim -2$ and a Kroupa IMF with $M_{\text{min}} = 0.1 M_\odot$ and $M_{\text{max}} = 100 M_\odot$, or a log-normal IMF around $M \sim 10 M_\odot$ with $\sigma_M \sim 1 M_\odot$ and with wide wings extending to $500 M_\odot$ (Raiter et al. 2010). However, the stellar contribution into ionizing (X-ray and EUV) photons can be neglected if $M_* \sim 0.02 M_*$.

2.4. Cumulative Incident Spectrum

As inferred for SMBHs in the local universe, their masses correlate with the stellar bulge of host galaxies (see reviews in Marconi & Hunt 2003; Häring & Rix 2004; Sani et al. 2011; Kormendi & Ho 2013; Heckman & Best 2014). In spite of a high spread (an order of magnitude, see, e.g., Kormendi & Ho 2013; Heckman & Best 2014) an approximate proportionality $M_*/M_* \sim 0.002$ (see Figure 18(b) in Kormendi & Ho 2013; Decarli et al. 2018) can be loosely accepted for low-redshift host galaxies. Observations of the [C] $158 \mu\text{m}$ line in a set of $z \gtrsim 6$ quasars led Walter et al. (2004) and Decarli et al. (2018) to conclude that the ratio M_*/M_* in SMBHs hosting galaxies at the $z \simeq 6\text{--}7$ epoch is an order of magnitude higher than the ratio in the local universe: $\langle M_*/M_* \rangle \sim 0.02$ at $z \sim 7$ versus 0.002 at $z \sim 0$, in conflict with a common scenario of coeval evolution of the stellar population and the central massive BH. This circumstance may either reflect more efficient growth of BHs compared to possibly quenched star formation, or correspond to the abovementioned OBG stages (Agarwal et al. 2013, 2016), with a relatively low stellar mass in host galaxies. In concordance with this we assume that a dominant fraction of baryons of host galaxies are in the form of a gaseous halo with mass $M_b = M_*/\alpha$, with $\alpha = 0.002$ as a fiducial value, thus making the gas a sufficient reservoir for the formation of stars at later epochs. The gas is assumed to homogeneously occupy a spherical layer with the density $n_i = 1 \text{ cm}^{-3}$, which is typical for a diffuse interstellar matter (ISM) in a virialized halo at $z \sim 20$ (e.g., Barkana & Loeb 2001). Thus, the spherical layer has a thickness equal to $\Delta R \sim M_b / (4\pi R^2 m_p n_i)$, where m_p is the proton mass, and R is the radius of a halo. The inner radius is kept fixed $r_{\text{in}} = 30 \text{ pc}$. In what follows we will restrict the mass of stellar population by the ratio $M_*/M_* \gtrsim 1$.

As mentioned above for such a high M_*/M_* , the BH with Eddington luminosity $L_{*,\text{bol}} \geq 1.3 \times 10^{38} (M_*/M_\odot)$ dominates the whole energy range from high-energy bands (X-ray, EUV) to optical and near and partly mid-infrared waves. For the stellar mass-to-luminosity ratio $M_*/L_* \sim 0.01 M_\odot/L_\odot$ typical for a top-heavy Population III IMF and even for $M_*/M_* = 0.02$, $L_{*,\text{bol}} \gtrsim 6L_*$. The far-infrared is dominated by stellar population; however, its overall energetics are negligible. Therefore, under such conditions the thermal and ionization state of the ISM of a host galaxy are totally determined by the radiation of the central growing BH. From this point of view the soft X-ray excess along with EUV photons from the intermediate accretion disk (Kubota & Done 2018) plays a crucially important role.

⁴ <http://www.astro.uu.se/~ez/yggdrasil/yggdrasil.html>

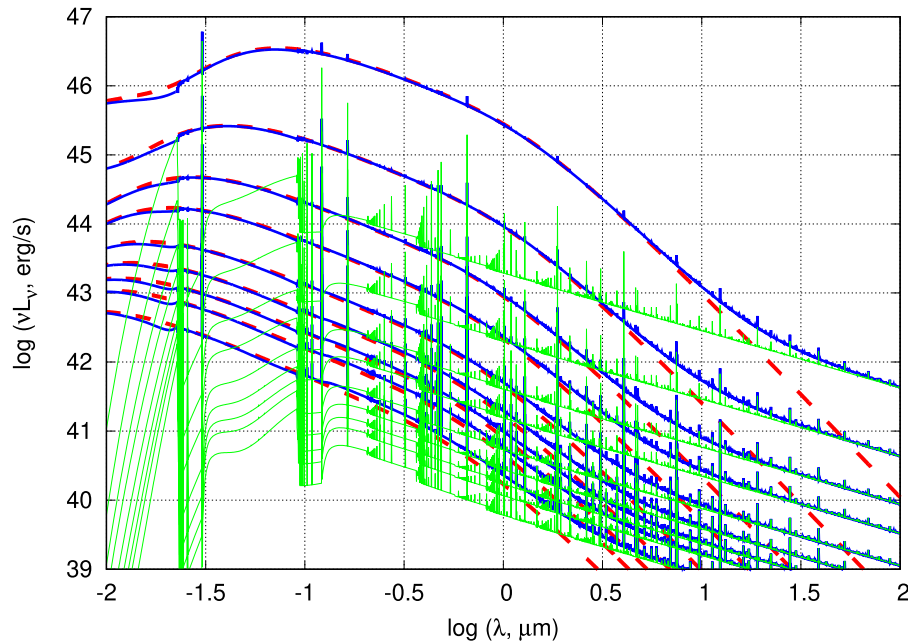


Figure 3. Incident continuum (red dashed lines), the net transmitted continuum, i.e., the sum of the attenuated incident and nebular continua along with spectral lines (blue thick lines), the nebular emission of hot gas in continuum and lines (green thin line) for the BH masses evolved following to Figure 1 for $z = 16-8$ with $\Delta z = 1$ (from bottom to top).

3. Results

3.1. Nebular Emission Spectra

Photons emitted by an accreting BH are transmitted through the surrounding gaseous layer. In the layer we assume photoionization and thermal equilibrium. We use CLOUDY (ver. 17, Ferland et al. 2017) to obtain the ionization composition and the transmitted spectrum. Figure 3 shows the incident continuum radiation (red lines), the nebular emission from the ionized gaseous layer in spectral lines and continuum (green lines), and the sum of the two (blue lines) for the BH masses evolved following Figure 1 for $z = 16-8$ with a step $\Delta z = 1$.

3.1.1. Line Emission

The strongest lines in the spectra presented in Figure 3 are the longest-wavelength lines of the hydrogen series: Ly α (1215 Å), H α (6563 Å), Pa α (1.875 μm), Br α (4.05 μm), Pf α (7.46 μm), Hu α (12.37 μm), H β , H γ , and He II 1640 Å. He II 1.01 μm are also worth mentioning. The lines are more clearly seen above the continuum for less massive BHs, although they remain recognizable (except only He II 1.01 μm line) even for the most massive BHs considered here. These lines can be used not only for measuring redshifts of BH host galaxies, but also for identification of the source as an OBG candidate. Their luminosities in optical lines ($\lambda < 1 \mu\text{m}$) exceed $10^{42} \text{ erg s}^{-1}$ for redshifts $z \lesssim 12$, and the thermal widths range in 25–35 km s^{-1} . Their fluxes in H α line can reach up to several μJy and as such may be detected even in the high-resolution spectral mode of the Near-Infrared Spectrograph⁵ installed on *JWST* (see e.g., Kalirai 2018). The IR lines may be resolved for massive BH grown in earlier epochs $z \gtrsim 9$ with line luminosities as high as $10^{42} \text{ erg s}^{-1}$. Indeed, for example, the expected flux in Pf α (7.46 μm) line being of order

$\sim 30 \mu\text{Jy}$, is higher than the detection limit for moderate spectral mode ($R = 1000$) of the planned space telescope Spektr-M (Millimetron, see in Kardashev et al. 2014). On the other hand the flux from even the most luminous BHs with a line luminosity, $\sim 10^{43} \text{ erg s}^{-1}$ at $z \sim 8$, as presented in Figure 3, is close to the low-resolution ($R = 300$) sensitivity threshold of the SAFARI spectrograph (as it was a part of the SPICA mission; see Spinoglio et al. 2017; Roelfsema et al. 2018).

3.1.2. Continuum

Numerical models of radially stratified accretion slim disks with a shallow radial luminosity profiles reveal a slightly weaker dependence of the effective disk temperature on the BH mass (Kubota & Done 2019) than the one predicted in the analytical Novikov–Thorne disk emissivity model. In Figure 2 the intrinsic spectrum of a BH in the long wavelength limit $\lambda > 1 \mu\text{m}$ behaves as a blackbody with the effective temperature $T_{\text{eff}} \propto M_*^{1.5}$

$$\mathcal{L}_\nu^* \equiv \nu L_{\nu,*} \simeq 6 \times 10^{46} M_{*,9}^{1.5} \lambda_1^{-3} \text{ erg s}^{-1}, \quad \lambda \geq 1 \mu\text{m}, \quad (3)$$

versus $T_{\text{eff}} \propto M_*^{1.8}$ for Novikov–Thorne emissivity (Novikov & Thorne 1973), where $M_{*,9} = M_*/10^9 M_\odot$, $\lambda_1 = \lambda/1 \mu\text{m}$.

Ionized and heated ISM gas emits a considerable fraction of the BH energy in free–free (bremsstrahlung) continuum. In the limit of long wavelengths, $\lambda \geq 0.3 \mu\text{m}$, it is (see Draine 2011)

$$\mathcal{L}_\nu^{\text{ff}} \equiv \nu L_\nu^{\text{ff}} \simeq 3.4 \times 10^{41} T_4^{-0.323} n_e M_{g,9} \lambda_1^{-0.882} \text{ erg s}^{-1}, \quad (4)$$

where the fractional ionization x in the emitting region is $x \simeq 1$, $M_{g,9} = M_g/10^9 M_\odot$ is gas mass, and $T_4 = T/10^4 \text{ K}$ is gas temperature.

When the interrelation between the gas and BH masses $M_g = 500 M_*$ is explicitly assumed (as for the case shown in Figure 3) the free–free nebular continuum overshines the intrinsic radiation from the BH at the wavelength $\lambda \geq \lambda_{1,k} \simeq 0.1 M_*^{0.26} \mu\text{m}$

⁵ <http://sci.esa.int/jwst/45694-nirspec-the-near-infrared-spectrograph/>

and the spectrum changes its slope—the “kink” in the spectrum. In the example shown in Figure 3 the wavelength of this “kink” $\lambda_k \simeq 15 \mu\text{m}$ for the SMBH with $M_* = 4 \times 10^8 M_\odot$ at $z = 8$. The corresponding luminosity at the kink is $\mathcal{L}_k \sim 5 \times 10^{42} \text{ erg s}^{-1}$, as seen in Figure 3; for an arbitrary z within this model: $\mathcal{L}_k \propto 5.6 \times 10^{35} M_*^{0.76} \text{ erg s}^{-1}$, where M_* is units of in solar mass.

The “kink” transition will be detected in the continuum of BHs with $M_* \gtrsim 10^8 M_\odot$ at $z \lesssim 9$ by future instruments, since the photometric flux $\nu F_\nu = (1+z)\mathcal{L}_k/(4\pi d_L^2) \simeq 8 \times 10^{-28} M_*^{0.86} \text{ W m}^{-2}$, where d_L is the luminosity distance. For instance, the flux limit for the imaging mode of the low-resolution SAFARI spectrometer (Spinoglio et al. 2017; Roelfsema et al. 2018) is around $10^{-20} \text{ W m}^{-2}$ for a 10 hr integration time at wavelength $\sim 100 \mu\text{m}$, where the “kink” takes place. However, spectral observations ($R = 100$) are less optimistic for the SPICA mission: $F_\nu \simeq 2.5 \times 10^{-12} \lambda_{1,\text{obs}}^{5.8} \mu\text{Jy}$, where $\lambda_{1,\text{obs}} = (1+z)\lambda_{1,k}$ is the observed “kink” wavelength in μm . For instance, the maximum flux $\sim 10 \mu\text{Jy}$ reached for $M_* \sim 8 \times 10^8 M_\odot$ at $z = 8$ is about 1.5 orders of magnitude lower than the limit detected by the SAFARI spectrometer within 10 hr integration time.

Generally, when the gas mass is a free parameter not connected to the BH mass, the transition from the bremsstrahlung with slope $\beta = 0.118$ to the quasi-blackbody spectrum with $\beta = 2$ occurs at λ_k depending on gas mass M_g . The two observables, the “kink” wavelength λ_k and the corresponding luminosity $\mathcal{L}_k \simeq 2\mathcal{L}_k^{\text{ff}}$ —allow us to derive the two different variables: M_* and M_g . The first follows immediately from Equation (3), while the second can be derived from Equation (4) when accounting for $\mathcal{L}_k \simeq 2\mathcal{L}_k^{\text{ff}}$ and that λ_k is linked to \mathcal{L}_k and M_* from Equation (3). Eventually, we arrive at the relation

$$M_* \sim \mathcal{L}_{k,47}^{0.68} \lambda_k^2, \quad (5)$$

and

$$M_g \sim 2 \times 10^5 n_e T_4^{-0.323} \mathcal{L}_{k,47}^{0.68} \lambda_k^{0.9}, \quad (6)$$

and correspondingly, all masses are given in $10^9 M_\odot$, $\mathcal{L}_{k,47} = \mathcal{L}_k/10^{47} \text{ erg s}^{-1}$.

4. Discussion

As mentioned above, an approximate proportionality between a central BH mass and stellar mass of galaxies hosting BHs in the local universe $M_*/M_* \sim 0.002$ (e.g., Kormendi & Ho 2013; Heckman & Best 2014; Decarli et al. 2018) tends to increase by an order of magnitude to higher redshifts (Walter et al. 2004; Decarli et al. 2018). This might indicate that a coeval interrelation between M_* and M_g was slightly shifted toward BHs in the earlier epochs, in the spirit of obese black hole galaxies, such that the galaxies’ gas components in BH host galaxies served as a reservoir for feeding BHs and forming stars. Within this assumption one may think that the gas mass in a host galaxy is one of the major factors determining the relation M_*/M_* over the course of evolution. The estimates given above were performed within this hypothetical scenario.

Figure 4 presents the luminosity in continuum L_k (upper panel) and the wavelength λ_k (lower panel) at the “kink,” where the free–free nebular emission overshines the BH quasi-blackbody versus the gas mass M_g exposed to a BH of fixed mass M_* . Increasing the gas mass for a fixed M_* results in a proportional increase of the nebular emission. The “kink”

wavelength λ_k is shifted shortward for a higher gas mass. The flat parts in L_k and λ_k curves correspond to a saturation of luminosity when the “kink” transition wavelength becomes close to the Lyman break, i.e., the nebular emission overshines the BH at wavelengths $\sim 1000 \text{ \AA}$ (see the red and green lines in Figure 4). The increase in gas density manifests in an increase of free–free continuum and a shortward shift of the “kink” transition wavelength (see the green dashed and solid lines in Figure 4). The increase of BH mass for the fixed gas mass leads to a shift of the “kink” transition wavelength longward where the free–free continuum is lower.

Interrelations between the expected fluxes and wavelengths shown in Figure 4 when the emitting objects are located at $z = 9$, are combined into Figure 5. Even for massive BHs $M_* \sim 10^8 M_\odot$ the flux is less than $\sim 1 \mu\text{Jy}$. Such flux lies at the sensitivity threshold for the imaging mode ($R = 3$, 1 hr integration) of the planned space telescope Spektr-M (see in Kardashev et al. 2014). For the SAFARI spectrometer, this flux is about 100 times below the limit. Note that the flux varies with gas mass as $\nu F_\nu \sim M_g^{1.5}$, and is weakly sensitive to its density.

The critical issue for the models considered here is the observability of SMBHs grown from DCBH seeds on the OBG phase. In addition to the question of their brightness, the key issue is how many such objects can be met in the field of view (FoV) of a telescope. Recent theoretical models predict the number density of DCBH at redshifts $z \sim 10\text{--}13$ in the range $n(z) \sim 10^{-7}\text{--}3 \times 10^{-6}$ per comoving Mpc^3 (Dijkstra et al. 2014; Wise et al. 2019). The SMBH mass function is expected to have a peak around $\sim 10^5 M_\odot$ (Basu & Das 2019). The most plausible SMBH fraction with $M_* \sim 10^7\text{--}10^8 M_\odot$ is $\gtrsim 0.03\text{--}0.1$ for an Eddington or supercritical growth regime (Basu & Das 2019). Thus, the number of SMBHs with $M_* \sim 10^7\text{--}10^8 M_\odot$ in the redshift range $z \sim 10\text{--}11$ is $N \sim 0.03\text{--}2$ objects per square arcmin. Thus, one would require less than 5 random pointings of the *JWST* FoV ($2' \times 2'$) for detection of at least one such object. For the planning Spektr-M project with a $6 \times 6'$ FoV, a handful of such objects can be met in even one pointing.

5. Summary

In this paper we calculated spectral features of growing massive black holes during the stages when the host galaxy stellar population is underdeveloped, with a mass not exceeding the black hole mass. We assumed that a black hole begins growing from a low-mass seed at early epochs ($z \gtrsim 20$). The feeding rate is assumed to be kept on average in the Eddington accretion regime in order to increase its mass from $M_* \sim 3 \times 10^8\text{--}10^9 M_\odot$ to the redshifts $z \simeq 7.5$, as observed (see, e.g., in Mortlock et al. 2011; Bañados et al. 2018; Decarli et al. 2018). We showed the following:

1. While growing the black hole spends a considerable fraction of its hard photons of X-ray and EUV bands to ionize and heat the interstellar gas of the host galaxy.
2. Interstellar gas reradiates the ionizing photons of the BH in the EUV, optical, and infrared bands in continuum and line emission, with intensities depending on the BH growing rate, and thus can serve as a diagnostic of its evolutionary stages.
3. At longer wavelengths, in the infrared and far-infrared bands, bremsstrahlung continuum reradiated by the ISM gas overshines the continuum from the BH, resulting in a

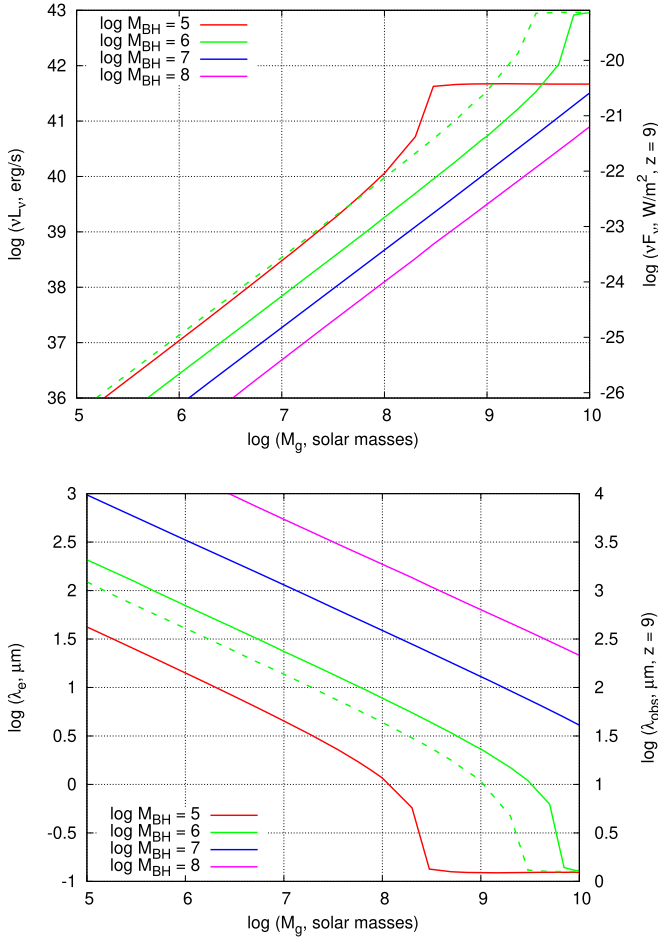


Figure 4. Luminosity at the “kink” \mathcal{L}_k (upper panel) and the “kink” wavelength λ_k (lower panel) vs. mass of the emitting gas layer for several values of BH mass M . (color lines). The solid lines show the models for $n = 1 \text{ cm}^{-3}$, and the dashed line depicts the model for $n = 3 \text{ cm}^{-3}$ and $M = 10^6 M_\odot$: it is seen that at a fixed gas mass \mathcal{L}_k and λ_k scale with gas density approximately as $\sim n^{0.4}$ and $\sim n^{-0.47}$, correspondingly, in accordance with the arguments in Section 3.1.2. The right axes correspond to the flux and the wavelength emitted at redshift $z = 9$.

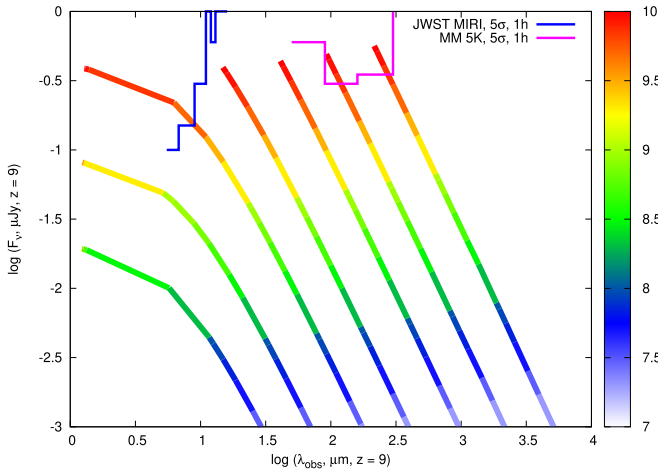


Figure 5. Wide-band (the spectral resolution $R = 100$) flux of free–free continuum at the kink λ_k emitted at redshift $z = 9$ for several values of BH mass M : 10^5 , $10^{5.5}$, 10^6 , $10^{6.5}$, 10^7 , $10^{7.5}$, $10^8 M_\odot$ from left to right; the color indicates the gas mass. The blue and pink lines depict the expected detection limits (1 hr integration) of the *JWST* MIRI and Spektr-M (MM) telescopes, correspondingly.

change of spectral index from a Rayleigh–Jeans like $\propto \lambda^{-2}$ at shorter wavelengths to the flat free–free $\lambda^{0.118}$ in the far-infrared. The wavelength corresponding to such a transition at $\lambda \sim \lambda_k$ and the luminosity \mathcal{L}_k can trace the BH evolutionary stage: the BH mass can be inferred as $M_*(z) \propto \mathcal{L}_k^{0.68} \lambda_k^2(z)$, the mass of the free–free emitting ISM gas is $M_g \propto \mathcal{L}_k^{0.68} \lambda_k^{0.9}$.

We thank the referee for a careful reading and helpful suggestions. We thank also I. Khrykin for introducing us to pythoning, and T. Larchenkova for discussing the effects of gravitational lensing. This work is supported by the joint RFBR-DST project (RFBR 17-52-45063, DST P-276). E.V. is grateful to the Ministry for Education and Science of the Russian Federation (grant 3.858.2017/4.6). The work of Y.S. was done under partial support from the joint RFBR-DST project (17-52-45053), by the project 01-2018 “New Scientific Groups LPI,” and the Program of the Presidium of RAS (project code 28).

ORCID iDs

Evgenii O. Vasiliev <https://orcid.org/0000-0001-5153-158X>
Yuri A. Shchekinov <https://orcid.org/0000-0002-3463-7339>

References

- Abramowicz, M. A., Czerny, B., Lasota, J. P., & Szuszkiewicz, E. 1988, *ApJ*, **332**, 646
- Agarwal, B., Davis, A. J., Khochfar, S., et al. 2013, *MNRAS*, **432**, 3438
- Agarwal, B., Smith, B., Glover, S., et al. 2016, *MNRAS*, **459**, 4209
- Alexander, T., & Natarajan, P. 2014, *Sci*, **345**, 1330
- Bañados, E., Venemans, B. P., Mazzucchelli, C., et al. 2018, *Natur*, **553**, 473
- Bañados, E., Venemans, B. P., Morganson, E., et al. 2014, *AJ*, **148**, 14
- Barkana, R., & Loeb, A. 2001, *PhR*, **349**, 125
- Barrow, K. S. S., Aykutaalp, A., & Wise, J. H. 2018, *NatAs*, **2**, 987
- Basu, S., & Das, A. 2019, *ApJL*, **879**, L3
- Begelman, M. C., & Meier, D. L. 1982, *ApJ*, **253**, 873
- Bolton, A. S., Burles, S., Koopmans, L. V. E., et al. 2008, *ApJ*, **682**, 964
- Bromm, V., & Loeb, A. 2003, *ApJ*, **596**, 34
- Chon, S., Hirano, S., Hosokawa, T., & Yoshida, N. 2016, *ApJ*, **832**, 134
- Decarli, R., Walter, F., Venemans, B. P., et al. 2018, *ApJ*, **857**, 97
- Dijkstra, M., Ferrara, A., & Mesinger, A. 2014, *MNRAS*, **442**, 2036
- Draine, B. T. 2011, *Physics of the Interstellar and Intergalactic Medium* (Princeton: Princeton Univ Press)
- Fan, X., Strauss, M. A., Schneider, D. P., et al. 2003, *AJ*, **125**, 1649
- Fan, X., Wang, F., Yang, J., et al. 2019, *ApJL*, **870**, L11
- Ferland, G. J., Chatzikos, M., Guzmán, F., et al. 2017, *RMxAA*, **53**, 385
- Fujimoto, S., Oguri, M., Nagao, T., Izumi, T., & Ouchi, M. 2019, arXiv:1909.13512
- Haehnelt, M. G., & Rees, M. J. 1993, *MNRAS*, **263**, 168
- Haiman, Z. 2013, in *The First Galaxies*, ed. T. Wiklind, B. Mobasher, & V. Bromm, 396 (Berlin: Springer), 293
- Haiman, Z., & Loeb, A. 2001, *ApJ*, **552**, 459
- Häring, N., & Rix, H. W. 2004, *ApJL*, **604**, L89
- Heckman, T. H., & Best, P. N. 2014, *ARA&A*, **52**, 589
- Inayoshi, K., Li, M., & Haiman, Z. 2018, *MNRAS*, **479**, 4017
- Izumi, T., Onoue, M., Matsuoka, Y., et al. 2019, *PASJ*, in press (arXiv:1904.07345)
- Johnson, J. L., & Bromm, V. 2007, *MNRAS*, **374**, 1557
- Kalirai, J. 2018, *ConPh*, **59**, 251
- Kardashev, N. S., Novikov, I. D., Lukash, V. N., et al. 2014, *PhyU*, **57**, 1199
- Kormendi, J., & Ho, L. C. 2013, *ARA&A*, **51**, 511
- Kubota, A., & Done, C. 2018, *MNRAS*, **480**, 1247
- Kubota, A., & Done, C. 2019, *MNRAS*, **489**, 524
- Latif, M. A., & Ferrara, A. 2016, *PASA*, **33**, 51
- Lodato, G., & Natarajan, P. 2006, *MNRAS*, **371**, 1813
- Madau, P., Haardt, F., & Dotti, M. 2014, *ApJL*, **784**, L38
- Madau, P., Rees, M. J., Volonteri, M., et al. 2004, *ApJ*, **604**, 484
- Madau, U., Borgani, S., Ciardi, B., & Petkova, M. 2019, *PASA*, **36**, 20
- Marconi, A., & Hunt, L. K. 2003, *ApJL*, **589**, L21

- Mortlock, D. J., Warren, S. J., Venemans, B. P., et al. 2011, *Natur*, 474, 616
- Natarajan, P., Pacucci, F., Ferrara, A., et al. 2017, *ApJ*, 838, 117
- Natarajan, P., Ricarte, A., Baldassare, V., et al. 2019, *BAAS*, 51, 73
- Novikov, I. D., & Thorne, K. 1973, in *Black Holes*, ed. C. de Witt & B. S. de Witt (London: Gordon and Breach), 345
- Pacucci, F., Ferrara, A., Grazian, A., et al. 2016, *MNRAS*, 459, 1432
- Pacucci, F., & Loeb, A. 2019a, *ApJL*, 870, L12
- Pacucci, F., & Loeb, A. 2019b, arXiv:1910.10156
- Pacucci, F., Natarajan, P., Volonteri, M., et al. 2017, *ApJL*, 850, L42
- Paczynski, B., & Abramowicz, M. A. 1982, *ApJ*, 253, 897
- Pei, Y. C. 1995, *ApJ*, 440, 485
- Raiter, A., Schaerer, D., & Fosbury, R. A. E. 2010, *A&A*, 523, 64
- Roelfsema, P. R., Shibai, H., Armus, L., et al. 2018, *PASA*, 35, e030
- Sani, E., Marconi, A., Hunt, L. K., & Risaliti, G. 2011, *MNRAS*, 413, 1479
- Shapiro, S. L. 2005, *ApJ*, 620, 59
- Soltan, A. 1982, *MNRAS*, 200, 115
- Spinoglio, L., Alonso-Herrero, A., Armus, L., et al. 2017, *PASA*, 34, e057
- Valiante, R., Schneider, R., Zappacosta, L., et al. 2018, *MNRAS*, 476, 407
- Visbal, E., Haiman, Z., & Bryan, G. L. 2014a, *MNRAS*, 442, L100
- Visbal, E., Haiman, Z., & Bryan, G. L. 2014b, *MNRAS*, 445, 1056
- Volonteri, M., Haardt, F., & Madau, P. 2003, *ApJ*, 582, 559
- Volonteri, M., Lodato, G., & Natarajan, P. 2008, *MNRAS*, 383, 1079
- Volonteri, M., & Rees, M. J. 2005, *ApJ*, 633, 624
- Volonteri, M., Silk, J., & Dubus, G. 2015, *ApJ*, 804, 148
- Walter, F., Carilli, C., Bertoldi, F., et al. 2004, *ApJL*, 615, L17
- Willott, C. J., Delorme, P., Reylé, C., et al. 2010, *AJ*, 139, 906
- Wise, J. H., Regan, J. A., O'Shea, B. W., et al. 2019, *Natur*, 566, 85
- Wu, X.-B., Wang, F., Fan, X., et al. 2015, *Natur*, 518, 512
- Yoo, J., & Miralda-Escude, J. 2004, *ApJL*, 614, L25
- Yoshida, N., Abel, T., Hernquist, L., et al. 2003, *ApJ*, 592, 645
- Zackrisson, E., Rydberg, C.-E., Schaerer, D., Östlin, G., & Tuli, M. 2011, *ApJ*, 740, 13